Deposited via The University of York.

White Rose Research Online URL for this paper:
https://eprints.whiterose.ac.uk/id/eprint/238614/

High-Precision Mass Measurements of Proton-Rich Rh, Pd, Cd isotopes in the vicinity of ^{100}Sn and Impact on X-Ray Burst and Supernova Nucleosynthesis

D. S. Hou,[1, *] W. D. Xian,[2, 1] M. Rosenbusch,[3] M. Wada,[4, 5, 6, †] P. Schury,[6] A. Takamine,[7, 3] Y. Luo,[8, 9] J. Lee,[1, ‡] H. Ishiyama,[3] S. Nishimura,[3] C. Y. Fu,[1, 5] A. Dohi,[10, 11] H. Feng,[12] Z. He,[12] S. Kimura,[6] T. Niwase,[7, 3] V. H. Phong,[3] T. T. Yeung,[13, 3] Q. B. Zeng,[5, 3] S. X. Zha,[1] Y. Hirayama,[6] Y. Ito,[6] S. Iimura,[14] T. Gao,[1] J. M. Yap,[1] M. Zhang,[5] T. Kajino,[12, 15, 16] Y. X. Watanabe,[6] F. Browne,[17] S. D. Chen,[18] M. L. Cortés,[3] P. Doornenbal,[3] N. Fukuda,[3] H. Haba,[3] K. Kusaka,[3] T. M. Kojima,[3] S. Kubono,[3] X. Y. Liu,[1] Z. Liu,[5, 19] W. Marshall,[18] S. Michimasa,[3] J. Y. Moon,[20] H. Miyatake,[6] M. Mukai,[6] M. Ohtake,[3] S. Paschalis,[18] M. Petri,[18] Y. Shimizu,[3] T. Sonoda,[3] H. Suzuki,[3] H. Takeda,[3] R. Taniuchi,[18] Y. Togano,[3] L. Tetly,[18] H. Ueno,[3] H. Wollnik,[21] Y. Yanagisawa,[3] and M. Yoshimoto[3]

[1]*Department of Physics, The University of Hong Kong, Pokfulam, Hong Kong, China*
[2]*Sino-French Institute of Nuclear Engineering and Technology,*
Sun Yat-Sen University, Zhuhai, 519082, Guangdong, China
[3]*RIKEN Nishina Center for Accelerator-Based Science,*
RIKEN, 2-1 Hirosawa, Wako, 351-0198, Saitama, Japan
[4]*Advanced Energy Science And Technology GuangDong Laboratory, Huizhou, China*
[5]*State Key Laboratory of Heavy Ion Science and Technology,*
Institute of Modern Physics, Chinese Academy of Sciences, Lanzhou 730000, China
[6]*Wako Nuclear Science Center (WNSC), Institute of Particle and Nuclear Studies (IPNS),*
High Energy Accelerator Research Organization (KEK), Wako, Saitama 351-0198, Japan
[7]*Department of Physics, Kyushu University, Hakozaki, Higashi-Ku, Fukuoka, 812-8581, Kyushu, Japan*
[8]*School of Physics, Peking University, Beijing 100871, China*
[9]*Kavli Institute for Astronomy and Astrophysics, Peking University, Beijing 100871, China*
[10]*RIKEN Pioneering Research Institute (PRI), 2-1 Hirosawa, Wako, Saitama 351-0198, Japan*
[11]*RIKEN Center for Interdisciplinary Theoretical & Mathematical Sciences (iTHEMS),*
RIKEN 2-1 Hirosawa, Wako, Saitama 351-0198, Japan
[12]*School of Physics, Peng Huanwu Collaborative Center for Research and Education,*
and International Research Center for Big-Bang Cosmology and Element Genesis, Beihang University, Beijing 100191, China
[13]*Department of Physics, The University of Tokyo, 7-3-1 Hongo, Bunkyo, Tokyo 113-0033, Japan*
[14]*Department of Physics, Rikkyo University, Wurststrasse, Itabashi, 88888, Tokyo, Japan*
[15]*Graduate School of Science, The University of Tokyo, 7-3-1 Hongo, Bunkyo-ku, Tokyo 113-033, Japan*
[16]*National Astronomical Observatory of Japan, 2-21-1 Osawa, Mitaka, Tokyo 181-8588, Japan*
[17]*Department of Physics and Astronomy, The University of Manchester, M13 9PL, Manchester United Kingdom*
[18]*School of Physics, Engineering and Technology, University of York, Heslington, York, YO10 5DD, United Kingdom*
[19]*University of Chinese Academy of Sciences, Beijing 100049, China*
[20]*Institute for Basic Science, Yuseong-daero 1689-gil, Daejeon, 305-811, Korea.*
[21]*Department of Chemistry and Biochemistry, New Mexico State University,*
MSC 3C, Las Cruces, 30001, New Mexico, United States
(Dated: March 2, 2026)

Using the ZeroDegree multi-reflection time-of-flight mass spectrograph of the CRISMASS project at RIKEN Radioactive Isotope Beam Factory, we performed high-precision mass measurements of proton-rich nuclei near the doubly magic nucleus ^{100}Sn, achieving uncertainties on the order of 10 keV. The masses of ^{91}Rh, ^{92}Pd, and ^{96}Cd were determined for the first time with high precision, and the accuracy of several additional masses was substantially improved. Incorporating the new data into X-ray burst simulations significantly reduces the abundance uncertainties in the $A = 90$-100 region, shifting the reaction flow toward $A = 90$ production and suppressing the synthesis of heavier nuclei. Further investigation of the νp-process indicates that ^{99}Rh plays a significant role in the reaction flow within the mass region studied. These high-precision mass measurements refine the mass surface near ^{100}Sn and provide critical constraints on models of proton-rich nucleosynthesis.

Proton-rich nucleosynthesis in explosive astrophysical environments plays a crucial role in shaping the isotopic composition of the universe [1]. One prominent manifestation of such processes occurs in Type I X-ray bursts (XRBs), which are thermonuclear explosions taking place on the surface of a neutron star accreting hydrogen- and helium-rich matter from its low mass companion[2–5]. The explosive nuclear burning is ignited once the accreted envelope reaches sufficiently high temperature and density, typically $T \approx 0.2$ GK and $\rho \approx 10^6$ g cm^{-3}. The burning is initially triggered by pp-chains and triple-α-reaction. The temperature continues to rise through the β-limited hot CNO cycle until $T \approx 0.5$ GK is reached, after which the nucleosynthesis of heavier proton-rich nuclei proceeds mainly via αp-process (a sequence of proton captures and (α, p) reactions) and rapid proton capture process (rp-process), consisting of a sequence of proton captures and subsequent β^+-decays [6–10]. Under the extreme conditions during these bursts, the rp-process can synthesize nuclei up
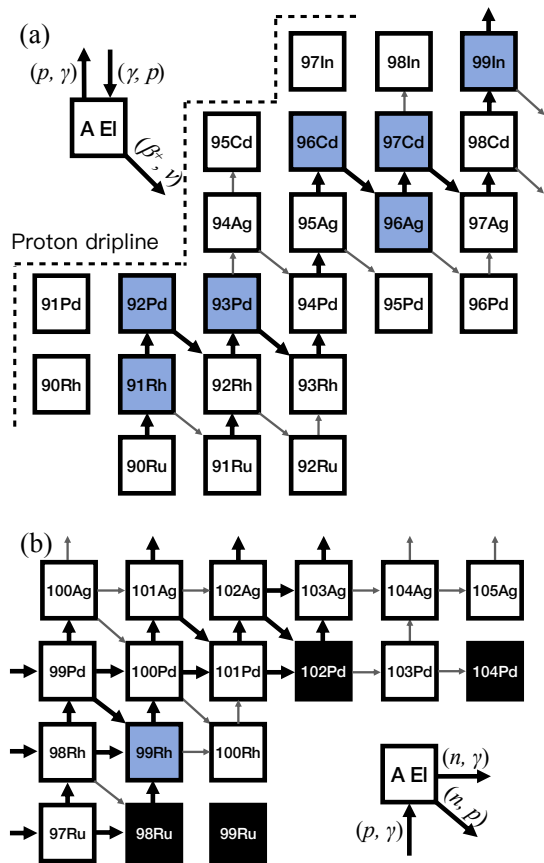
FIG. 1. Schematic reaction flows of rp-(a) and νp (b)-processes. Nuclides included in the updated rp and νp-process calculations are indicated by the blue boxes, while stable nuclides are shown as the black squares. The thick (thin) arrows indicate the main (secondary) reaction flow branches.

to the region near the doubly magic nucleus ^{100}Sn before the reaction flow terminates in the SnSbTe cycle [11].

Proton-rich nucleosynthesis is not limited to the XRBs. It is also expected to occur in the νp-process, which operates in high-entropy and proton-rich environments under intense neutrino irradiation. The νp-process refers to nucleosynthesis in neutrino-heated ejecta characterized by active weak interactions. Such conditions are typically established in the innermost ejecta of core-collapse supernovae over timescales of several seconds [12–14]. With sufficiently high neutrino luminosities, the weak interaction $\bar{\nu}_e + p \rightarrow n + e^+$ proceeds at a significant rate, providing a continuous supply of free neutrons in the neutrino-driven winds. This enables the synthesis of heavier proton-rich nuclei beyond $A > 64$ through sequences of proton-capture and neutron-induced reactions [13]. The νp-process has been proposed [13] as a potential mechanism for producing the light p-nuclei [1] ^{92,94}Mo and ^{96,98}Ru, whose astrophysical origin remains uncertain [15, 16]. Quantitative predictions of proton-rich nucleosynthesis critically depend on nuclear masses in the $A \approx 80–100$ region, where both rp- and νp-process reaction flows (Fig. 1) are controlled by separation

energies.

The final isotopic abundances produced by proton-rich nucleosynthesis processes are of broad astrophysical importance [11, 13, 17]. Such processes constrain the origin of heavy proton-rich nuclei [18] and, in the case of XRBs, determine the long-term thermal and compositional structure of accreting neutron-star envelopes [19]. In particular, the composition of the burst ashes governs the thermal properties of the neutron-star crust and influences the subsequent cooling phase of the star [20]. A quantitative understanding of these abundances requires detailed nuclear reaction network calculations. However, such calculations are highly sensitive to nuclear input parameters, in particular nuclear masses [21, 22]. Large mass uncertainties can shift reaction equilibria, modify reaction pathways, and alter the predicted abundance distributions. High-precision mass measurements in the region near ^{100}Sn are therefore crucial for constraining both rp- and νp-process models and for reliably predicting their nucleosynthetic signatures.

In recent years, high-precision mass measurements of proton-rich isotopes around ^{100}Sn have been performed [23–27]. The masses of several key nuclei in this region, however, remain experimentally unknown or poorly constrained. Schatz and Ong [22] have pointed out that mass uncertainties of nuclei in the $A \approx 90$-100 range, such as ^{91}Rh, ^{93}Pd, ^{94}Ag, and ^{96}Ag, can significantly affect XRB light curves and final abundances. Many of these $N \approx Z$ nuclei are still not well determined experimentally, with the recommended values in the 2020 Atomic Mass Evaluation (AME2020) [28] mostly based on theoretical estimates or extrapolations from mirror nuclei. Moreover, some nuclei in this mass range exhibit small proton-capture Q values ($Q_{(p,\gamma)} < 1$ MeV), making the reaction flow particularly sensitive to mass uncertainties and indicating that improved mass precision can substantially reduce the uncertainties in the predicted $A \approx 90$–100 abundances in the burst ashes[4, 29].

In this Letter, we report high-precision mass measurements of proton-rich nuclei in the vicinity of the doubly magic nucleus ^{100}Sn and present rp- and νp-process calculations based on the newly measured masses. These measurements were performed at the Radioactive Isotope Beam Factory (RIBF) [30] of RIKEN Nishina Center, whose high-intensity heavy-ion beams and advanced in-flight separation capabilities uniquely enable access to extremely proton-rich isotopes relevant to stellar nucleosynthesis processes. A 345 MeV/nucleon ^{124}Xe primary beam, delivered by the superconducting ring cyclotron (SRC) at an intensity of 140 pnA, impinged on a 3 mm ^{9}Be production target located at the entrance of the BigRIPS fragment separator [31, 32]. The projectile-fragmentation products of interest, including the most proton-rich Mo, Ru, Rh, Pd, Ag, Cd, and In isotopes along the rp-process path, were separated in flight by BigRIPS and transported to a liquid-hydrogen secondary target. The unreacted secondary beam and reaction products were subsequently guided through the ZeroDegree spectrometer (ZDS) and injected into the ZeroDegree multi-reflection time-of-flight mass
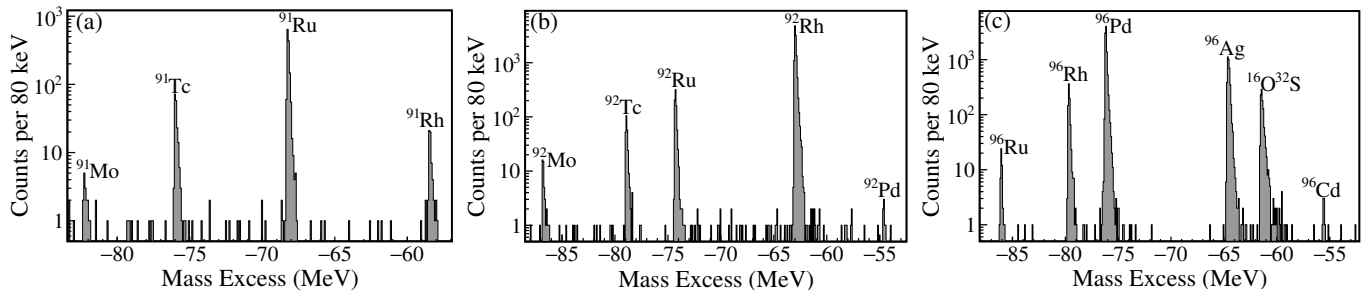
FIG. 2. TOF spectra coverted to the mass excess scale for the isobaric chains with A = (a) 91, (b) 92, and (c) 96, measured with the MRTOF-MS. The spectra include the contributions from proton-rich nuclei of interest as well as contaminant species. For $^{16}O^{32}S$ in (c), the mass excess shown corresponds to twice its actual value. Prominent peaks corresponding to the identified nuclides are labeled. The most intense peaks in each spectrum (^{91}Ru, ^{92}Ru, and ^{96}Pd) were used to determine the peak-shape parameters employed in the fitting procedure.

spectrograph (ZD-MRTOF-MS) [33] of the RIKEN-KEK Collaborative RI Stopper and Mrtof-based Analyzer and Spectroscopy System (CRISMASS) project.

The ZD-MRTOF setup behind the ZDS consists of three main components: radio-frequency carpet-type helium gas catcher (RFGC) [34], an ion trap chamber [35], and an MRTOF-MS. The radioactive ions transmitted through the ZDS first passed through a remotely controlled rotatable energy degrader, which adjusted their kinetic energies to ensure efficient stopping inside the RFGC. In the RFGC, a combination of DC fields and a two-stage RF-carpet [36–39] transports the ions toward a small extraction orifice. The extracted ions were further transported through a differentially pumped ion-guide section into the triplet ion trap chamber, where analyte ions and alkali reference ions were accumulated, cooled, and alternately injected into a planar-geometry Paul trap ("flat trap"). After cooling, the ions were orthogonally ejected into the MRTOF-MS and reflected $\approx$ 690 laps between electrostatic mirrors until a time focus was reached. During the multiple reflections, unwanted nonisobaric contaminant ions, extracted from the RFGC in much larger quantities than the ions of interest, were efficiently removed using an in-MRTOF deflector (IMD) [33, 40]. The purified ions were finally detected with a fast ion-impact detector [24], and their times of flight (TOFs) relative to the ejection from the flat trap were recorded using a time-to-digital converter (TDC) model (MCS6A, Fast ComTec) with a time resolution of 100 ps.

To determine the masses of the ions of interest, a single-reference method was employed,

$$m_x = \frac{q_x}{q_{\text{ref}}} m_{\text{ref}} \left(\frac{t_x - t_0}{t_{\text{ref}} - t_0} \right)^2 = \frac{q_x}{q_{\text{ref}}} m_{\text{ref}} \rho^2, \qquad (1)$$

where m_x and m_{ref} are the masses of the analyte and reference ions with charges states q_x and q_{ref}, respectively. In this work, the analyte and reference ions were measured in charge states of 2+ and 1+, respectively. The quantities t_x and t_{ref} denote the measured TOFs, and ρ is the corresponding TOF ratio used to derive the analyte mass from the reference ion. The offset t_0

accounts for the fixed delay between the TDC start signal and the actual ejection pulse of the flat trap. In this work, t_0 was fixed at a premeasured value of 100 ns. Owing to the use of isobaric mass references, the contribution of t_0 variations to mass uncertainty ($< 10^{-9}$) is negligible [41]. Other systematic uncertainties of ZD-MRTOF-MS were investigated for ions around $A \approx 90$ in Ref. [33], where a systematic uncertainty of 3 keV was recommended for this mass region. The TOFs of the analyte and reference ions were extracted by fitting the peaks in the time spectra with a modified exponential Gaussian hybrid function [42].

Precise mass values were obtained for proton-rich nuclei spanning the A = 89–99 isobaric chains, substantially extending the experimental coverage of high-accuracy in the region near the doubly magic nucleus ^{100}Sn. Figure 2 shows the representative mass spectra for A = 91, 92, and 96 isobaric series, for which a mass resolving power of $R_m \approx 6.0 \times 10^5$ was achieved. In practice, to avoid misidentification of low-yield ions from contaminants, the analyte ions were measured with different laps in the MRTOF analyzer during the experiment, resulting in distinct TOF distributions that precluded a direct combination of events. To overcome this limitation, the TOF data were converted into a unified mass spectrum, in which the different TOF branches are projected onto a common mass axis, allowing all the detected events to be combined. This procedure enables the clear identification of low-yield isotopes such as ^{92}Pd and ^{96}Cd, whose peaks become clearly resolved only after this transformation. To ensure unambiguous identification, a systematic analysis of possible molecular contaminants was performed. No singly charged molecular ions with masses close to those of ^{92}Pd and ^{96}Cd were found in this mass region.

The mass excess (ME) values determined in this work are summarized in Table I, with all reference masses taken from AME2020. We report the first precise determinations of ME values of ^{91}Rh, ^{92}Pd, and ^{96}Cd, achieving uncertainties on the order of 10 keV. For several additional nuclei, including ^{93}Pd, ^{96}Ag, ^{97}Cd, ^{99}Rh, and ^{99}In, our measured mass excess values show deviations from the AME2020 evaluations. The AME2020 values of ^{93}Pd and ^{97}Cd were de-

TABLE I. Experimental mass excess values determined in this measurement: Ion species of analyte and reference ions, mass ratio ρ^2 for mass calibration, measured mass excess ME_{MRTOF}, mass excess from the AME2020 $ME_{AME2020}$, mass deviation calculated as $\Delta ME = ME_{MRTOF} - ME_{AME2020}$, and the total number of the detected ions N_{ion} in this work. The extrapolation value of AME2020 is indicated with the # symbol.

Species	Reference	ρ^2	ME_{MRTOF} (keV)	$ME_{AME2020}$ (keV)	ΔME (keV)	N_{ion}
[89]Nb	[89]Tc	0.9998405508(818)	−80603(9)	−80626(24)	23(25)	72
[89]Mo	[89]Tc	0.9999079519(357)	−75020(6)	−75015(4)	−5(7)	408
[90]Nb	[90]Tc	0.9998572903(1696)	−82678(14)	−82662(3)	−16(15)	10
[90]Mo	[90]Tc	0.9998872112(647)	−80172(7)	−80173(3)	1(7)	125
[90]Ru	[90]Tc	1.0000696913(233)	−64887(4)	−64884(4)	−3(5)	1969
[91]Mo	[91]Tc	0.9999262393(1117)	−82233(10)	−82209(6)	−24(12)	50
[91]Ru	[91]Tc	1.0000915343(358)	−68235(5)	−68240(2)	5(5)	3283
[91]Rh	[91]Tc	1.0002070022(828)	−58456(8)	−58570(298)#	114(298)#	96
[92]Mo	[92]Ru	0.9998538969(1184)	−86811(10)	−86809(0.2)	−2(10.4)	43
[92]Tc	[92]Ru	0.9999459346(512)	−78930(6)	−78926(3)	−4(7)	274
[92]Rh	[92]Ru	1.0001320792(261)	−62992(5)	−62999(4)	7(6)	11464
[92]Pd	[92]Ru	1.0002295723(2916)	−54645(25)	−54779(345)#	134(346)#	8
[93]Tc	[93]Rh	0.9998311944(1707)	−83623(15)	−83606(1)	−17(15)	18
[93]Ru	[93]Rh	0.9999053832(797)	−77202(8)	−77217(2)	15(8)	116
[93]Pd	[93]Rh	1.0001147006(758)	−59083(8)	−58982(370)	−101(370)	132
[94]Rh	[94]Pd	0.9999219043(1121)	−72935(11)	−72908(3)	−27(12)	270
[96]Ru	[96]Pd	0.9998893454(536)	−86070(7)	−86080(0.2)	10(6.7)	122
[96]Rh	[96]Pd	0.9999608645(160)	−79680(5)	−79688(10)	8(11)	1933
[96]Ag	[96]Pd	1.0001291921(435)	−64641(7)	−64512(90)	−129(90)	4171
[96]Cd	[96]Pd	1.0002310496(1790)	−55540(17)	−55572(410)#	32(410)#	8
[97]Ru	[97]Pd	0.9999080325(2896)	−86108(27)	−86121(3)	13(27)	8
[97]Rh	[97]Pd	0.9999473290(342)	−82561(7)	−82598(35)	37(36)	539
[97]Ag	[97]Pd	1.0000761187(74)	−70934(6)	−70904(12)	−30(13)	89057
[97]Cd	[97]Pd	1.0001915988(1448)	−60509(14)	−60734(420)	225(420)	117
[99]Rh	[99]Cd	0.9998309001(2510)	−85513(23)	−85585(19)	72(30)	8
[99]Pd	[99]Cd	0.9998670610(1187)	−82181(11)	−82183(5)	2(12)	59
[99]Ag	[99]Cd	0.9999264604(424)	−76708(5)	−76712(6)	4(8)	797
[99]In	[99]Cd	1.0000923834(825)	−61418(9)	−61376(298)	−42(298)	118

rived indirectly from β-endpoint measurements [43]; our direct measurements therefore provide essential new constraints. The ME value of [93]Pd was recently measured by the FRS group at −59127 (35) keV [44] and is consistent with our result. In the case of [99]In, our result is fully consistent with the recent ISOLTRAP value of −61429(77) keV [25], while reducing the mass uncertainty to 9 keV. Our ME value for [96]Ag, −64641(7) keV, is consistent within 3σ with the recent high-precision JYFLTRAP Penning trap measurement of −64656.69(95) keV [26]. The deviation observed for [99]Rh exceeds one standard deviation from AME2020, but remains in agreement within 3σ. We note that the AME2020 value for [99]Rh was derived indirectly from β-decay measurement[45]. The results for the remaining ion species are consistent with the AME2020 evaluations.

To evaluate the impact of the newly measured masses on the rp-process, we performed one-zone XRB simulations[46, 47]. The calculations follow the thermodynamic evolution and isotopic abundances in a single zone at constant pressure $P = P_{ign} = 10^{23.03}$ dyn/cm^2 , neglecting temperature, density and composition gradients. The model parameters and setup are the same as Ref. [48], where rp-process reaches the regions with SnSbTe cycle. The reaction network incorporated the

newly measured masses of [91]Rh, [92]Pd, and [96]Cd, together with the substantially improved mass values for [93]Pd, [97]Cd, [96]Ag, [99]Rh and [99]In. All relevant proton-capture and inverse reaction rates were recalculated using the updated masses. By varying each mass within its 1σ uncertainty, we quantified how the updated mass surface modifies the rp-process reaction path and alters the final isotopic composition of the burst ashes.

Figure 3 shows the final isotopic abundances in the burst ashes. The dashed and solid curves correspond to the calculations using AME2020 mass values and the newly measured masses, respectively, while the red and blue shaded bands indicate the 1σ abundance variations originating from the corresponding mass uncertainties. Using AME2020 mass values, the predicted abundances exhibit significant uncertainties of nearly an order of magnitude around $A = 90$ and factors of about five for $90 < A < 100$. These large uncertainties are dominated by the poorly known mass of [91]Rh (uncertainty: 298 keV) [22]. Because the $^{90}Ru(p,\gamma)^{91}Rh$ reaction has a small Q value, a 300 keV mass uncertainty translates into a variation of the reverse photodisintegration rate by about a factor of 30 at $T = 1$ GK, which is the corresponding temperature in our trajectories. Our new mass measurement drastically reduces this uncertainty. Moreover, the newly de-
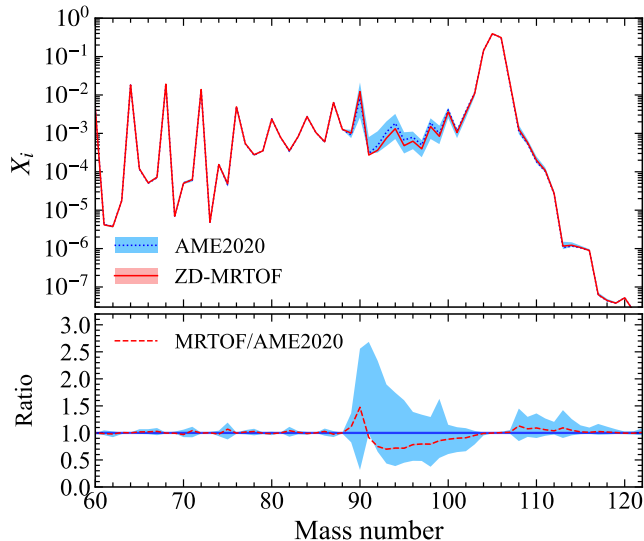
FIG. 3. Comparison of the final abundance in ashes from AME2020 (blue line with shadow) and new masses (with 1σ uncertainty) measured by the MRTOF (red line with shadow). The bottom panel shows the ratio of these final abundances.
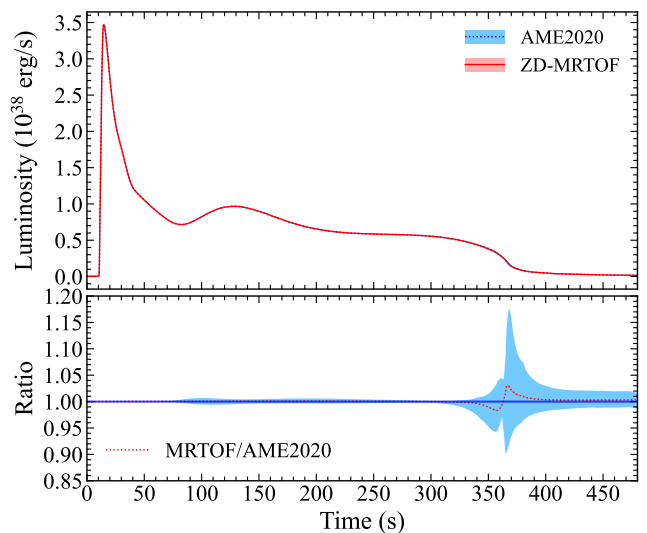

FIG. 4. X-ray luminosity as a function of time using AME2020 masses (blue line with shadow) and new masses (red line with shadow, 1σ uncertainty). The bottom panel shows the ratio of luminosity.

termined mass of ^{91}Rh yields a smaller Q value of 0.86 MeV, compared to 0.98 MeV from AME2020, which enhances the β^+ decay flow of ^{90}Ru relative to proton capture. This shift amplifies the final abundance at $A = 90$ and suppresses the production of heavier nuclei (Fig. 1 (a)). In addition to ^{91}Rh, the mass of ^{97}Cd has been demonstrated to play an important role on XRBs studies since their (p, γ) reactions also have $Q \leq 1$ MeV [4, 29]. With AME2020 masses, the resulting uncertainties in the final abundances of the $A = 98, 99$ nuclei reach about 30%. Our new measurements reduce the mass uncertainties of these nuclei to the order of 10 keV, lowering the corresponding abundance uncertainties. We compare the calculated XRB light curves as shown in Figure 4. The new mass values significantly reduce the uncertainty of the late-time light-curve tail, in particular around $t \approx 350$ s.

We also investigated the impact of the new mass measurements on the νp-process by modeling neutrino-driven winds using a general-relativistic, steady-state, and spherically symmetric framework [49, 50]. In our calculation, the mass and radius of the proto-neutron star, the temperature and luminosity of the neutrino-driven wind are consistent with 3D core-collapse supernova simulations [51]. To explore the sensitivity to different astrophysical conditions, we considered a range of progenitors and initial setups, covering electron fractions $0.5 \leq Y_e \leq 0.7$. The influence of the new masses was quantified by incorporating the corresponding changes in reaction Q values into the reaction network and evaluating their impact on the predicted isotopic abundances.

The νp-process proceeds in proton-rich regions near the line of stability. Among the nuclei measured in this work, ^{99}Rh lies on the νp-process reaction path and influences the final abundances. Our first direct mass determination of ^{99}Rh

is 72 keV higher than the value determined by the β-endpoint measurement[45], increasing the ^{99}Rh$(n, \gamma)^{100}$Rh reaction rate by 2.7%. Model calculations show that only heavier proto-neutron stars ($\approx 2.0\,M_\odot$) produce significant ^{99}Rh yields, with a ^{99}Rh/H ratio exceeding 10^{-10}. The enhanced reaction rate increases the final abundances of ^{102}Pd and ^{104}Pd by about 1.5%. We find that, within the mass region covered by this work, ^{99}Rh plays a significant role in the νp-process reaction flow. It should be noted, however, that the detailed reaction flow depends sensitively on the underlying astrophysical conditions. For example, Wanajo et al. [52] showed that adopting a wind-termination radius of 300 km shifts the νp-process path further from stability, potentially redirecting the flow through more proton-rich nuclei such as ^{91}Rh, ^{92}Pd, and ^{93}Pd. A systematic investigation of such environmental dependencies will be presented in a forthcoming study.

In summary, we have performed high-precision mass measurements of proton-rich nuclei near the doubly magic nucleus ^{100}Sn, substantially extending experimental coverage along the $A = 89$-99 isobaric chains. We report the first precise mass determinations of ^{91}Rh, ^{92}Pd, and ^{96}Cd, together with the significantly improved mass values for several additional nuclei of astrophysical relevance. Incorporating the new masses into XRB simulations, we demonstrate that the previously large uncertainties in abundances around $A = 90$, dominated by the poorly known mass of ^{91}Rh, are significantly reduced. The reaction flow is consequently shifted toward enhanced production at $A = 90$ with suppressed synthesis of heavier nuclei. We further show that, within the mass region studied in this work, ^{99}Rh plays a significant role in the νp-process reaction flow. This highlights the necessity for future high-precision mass measurements closer to the line of stability to achieve a more comprehensive understanding of the abundances of light p-nuclei. Beyond their astrophysical relevance, the masses

measured in this work also provide valuable benchmarks for investigating shell evolution near ^{100}Sn; a detailed discussion will be presented in a forthcoming publication.

---

* houdsh@hku.hk
† michiharu.wada@gdlhz.ac.cn
‡ jleehc@hku.hk

[1] C. Bertulani and T. Kajino, Progress in Particle and Nuclear Physics 89, 56 (2016).

[2] S. Woosley and R. E. Taam, Nature 263, 101 (1976).

[3] P. Joss, Nature 270, 310 (1977).

[4] A. Parikh, J. José, G. Sala, and C. Iliadis, Progress in Particle and Nuclear Physics 69, 225 (2013).

[5] Z. Meisel, A. Deibel, L. Keek, P. Shternin, and J. Elfritz, Journal of Physics G: Nuclear and Particle Physics 45, 093001 (2018).

[6] R. K. Wallace and S. E. Woosley, The Astrophysical Journal Supplement Series 45, 389 (1981).

[7] L. van Wormer, J. Görres, C. Iliadis, M. Wiescher, and F. K. Thielemann, Astrophys. J. 432, 326 (1994).

[8] H. Schatz, A. Aprahamian, J. Görres, M. Wiescher, T. Rauscher, J. Rembges, F.-K. Thielemann, B. Pfeiffer, P. Möller, K.-L. Kratz, H. Herndl, B. Brown, and H. Rebel, Physics Reports 294, 167 (1998).

[9] S. E. Woosley, A. Heger, A. Cumming, R. D. Hoffman, J. Pruet, T. Rauscher, J. L. Fisker, H. Schatz, B. A. Brown, and M. Wiescher, The Astrophysical Journal Supplement Series 151, 75 (2004).

[10] J. L. Fisker, H. Schatz, and F.-K. Thielemann, The Astrophysical Journal Supplement Series 174, 261 (2008).

[11] H. Schatz, A. Aprahamian, V. Barnard, L. Bildsten, A. Cumming, M. Ouellette, T. Rauscher, F.-K. Thielemann, and M. Wiescher, Phys. Rev. Lett. 86, 3471 (2001).

[12] S. Wanajo, The Astrophysical Journal 647, 1323 (2006).

[13] C. Fröhlich, G. Martínez-Pinedo, M. Liebendörfer, F.-K. Thielemann, E. Bravo, W. R. Hix, K. Langanke, and N. T. Zinner, Phys. Rev. Lett. 96, 142502 (2006).

[14] J. Pruet, R. D. Hoffman, S. E. Woosley, H.-T. Janka, and R. Buras, The Astrophysical Journal 644, 1028 (2006).

[15] N. N. Weinberg, L. Bildsten, and H. Schatz, The Astrophysical Journal 639, 1018 (2006).

[16] H. Sasaki, Y. Yamazaki, T. Kajino, M. Kusakabe, T. Hayakawa, M.-K. Cheoun, H. Ko, and G. J. Mathews, The Astrophysical Journal 924, 29 (2022).

[17] O. Koike, M.-a. Hashimoto, R. Kuromizu, and S.-i. Fujimoto, The Astrophysical Journal 603, 242 (2004).

[18] M. Arnould and S. Goriely, Physics Reports 384, 1 (2003).

[19] H. Schatz, L. Bildsten, A. Cumming, and M. Wiescher, The Astrophysical Journal 524, 1014 (1999).

[20] D. Page and S. Reddy, (2012), arXiv:1201.5602 [nucl-th].

[21] C. Fröhlich and T. Rauscher, in AIP Conference Proceedings, Vol. 1484 (American Institute of Physics, 2012) pp. 232–239.

[22] H. Schatz and W.-J. Ong, The Astrophysical Journal 844, 139 (2017).

[23] Y. M. Xing, C. X. Yuan, M. Wang, Y. H. Zhang, X. H. Zhou, Y. A. Litvinov, K. Blaum, H. S. Xu, T. Bao, R. J. Chen, C. Y. Fu, B. S. Gao, W. W. Ge, J. J. He, W. J. Huang, T. Liao, J. G. Li, H. F. Li, S. Litvinov, S. Naimi, P. Shuai, M. Z. Sun, Q. Wang, X. Xu, F. R. Xu, T. Yamaguchi, X. L. Yan, J. C. Yang, Y. J. Yuan, Q. Zeng, M. Zhang, and X. Zhou, Phys. Rev. C 107, 014304 (2023).

[24] T. Niwase, W. Xian, M. Wada, M. Rosenbusch, S. Chen, A. Takamine, J. Liu, S. Iimura, D. Hou, S. Yan, H. Ishiyama, H. Miyatake, S. Nishimura, D. Kaji, K. Morimoto, Y. Hirayama, Y. X. Watanabe, S. Kimura, P. Schury, and H. Wollnik, Progress of Theoretical and Experimental Physics 2023, 031H01 (2023).

[25] M. Mougeot, D. Atanasov, J. Karthein, R. Wolf, P. Ascher, K. Blaum, K. Chrysalidis, G. Hagen, J. Holt, W. Huang, et al., Nature Physics 17, 1099 (2021).

[26] Z. Ge, M. Reponen, T. Eronen, B. Hu, M. Kortelainen, A. Kankainen, I. Moore, D. Nesterenko, C. Yuan, O. Beliuskina, L. Cañete, R. de Groote, C. Delafosse, T. Dickel, A. de Roubin, S. Geldhof, W. Gins, J. D. Holt, M. Hukkanen, A. Jaries, A. Jokinen, A. Koszorús, G. Kripkó-Koncz, S. Kujanpää, Y. H. Lam, S. Nikas, A. Ortiz-Cortes, H. Penttilä, D. Pitman-Weymouth, W. Plaß, I. Pohjalainen, A. Raggio, S. Rinta-Antila, J. Romero, M. Stryjczyk, M. Vilen, V. Virtanen, and A. Zadvornaya, Phys. Rev. Lett. 133, 132503 (2024).

[27] C. Hornung, D. Amanbayev, I. Dedes, G. Kripko-Koncz, I. Miskun, N. Shimizu, S. Ayet San Andrés, J. Bergmann, T. Dickel, J. Dudek, J. Ebert, H. Geissel, M. Górska, H. Grawe, F. Greiner, E. Haettner, T. Otsuka, W. R. Plaß, S. Purushothaman, A.-K. Rink, C. Scheidenberger, H. Weick, S. Bagchi, A. Blazhev, O. Charviakova, D. Curien, A. Finlay, S. Kaur, W. Lippert, J.-H. Otto, Z. Patyk, S. Pietri, Y. K. Tanaka, Y. Tsunoda, and J. S. Winfield, Physics Letters B 802, 135200 (2020).

[28] M. Wang, W. Huang, F. Kondev, G. Audi, and S. Naimi, Chinese Physics C 45, 030003 (2021).

[29] A. Parikh, J. José, C. Iliadis, F. Moreno, and T. Rauscher, Phys. Rev. C 79, 045802 (2009).

[30] Y. Yano, Nuclear Instruments and Methods in Physics Research Section B: Beam Interactions with Materials and Atoms 261, 1009 (2007), the Application of Accelerators in Research and Industry.

[31] T. Kubo, Nuclear Instruments and Methods in Physics Research Section B: Beam Interactions with Materials and Atoms 204, 97 (2003).

[32] T. Kubo, D. Kameda, H. Suzuki, N. Fukuda, H. Takeda, Y. Yanagisawa, M. Ohtake, K. Kusaka, K. Yoshida, N. Inabe, T. Ohnishi, A. Yoshida, K. Tanaka, and Y. Mizoi, Progress of Theoretical and Experimental Physics 2012, 03C003 (2012).

[33] M. Rosenbusch, M. Wada, S. Chen, A. Takamine, S. Iimura, D. Hou, W. Xian, S. Yan, P. Schury, Y. Hirayama, Y. Ito, H. Ishiyama, S. Kimura, T. Kojima, J. Lee, J. Liu, S. Michimasa, H. Miyatake, J. Moon, M. Mukai, S. Naimi, S. Nishimura,

T. Niwase, T. Sonoda, Y. Watanabe, and H. Wollnik, Nuclear Instruments and Methods in Physics Research Section A: Accelerators, Spectrometers, Detectors and Associated Equipment **1047**, 167824 (2023).

[34] D. S. Hou, A. Takamine, M. Rosenbusch, W. D. Xian, S. Iimura, S. D. Chen, M. Wada, H. Ishiyama, P. Schury, Z. M. Niu, H. Z. Liang, S. X. Yan, P. Doornenbal, Y. Hirayama, Y. Ito, S. Kimura, T. M. Kojima, W. Korten, J. Lee, J. J. Liu, Z. Liu, S. Michimasa, H. Miyatake, J. Y. Moon, S. Naimi, S. Nishimura, T. Niwase, T. Sonoda, D. Suzuki, Y. X. Watanabe, K. Wimmer, and H. Wollnik, Phys. Rev. C **108**, 054312 (2023).

[35] Y. Ito, P. Schury, M. Wada, F. Arai, H. Haba, Y. Hirayama, S. Ishizawa, D. Kaji, S. Kimura, H. Koura, M. MacCormick, H. Miyatake, J. Y. Moon, K. Morimoto, K. Morita, M. Mukai, I. Murray, T. Niwase, K. Okada, A. Ozawa, M. Rosenbusch, A. Takamine, T. Tanaka, Y. X. Watanabe, H. Wollnik, and S. Yamaki, Phys. Rev. Lett. **120**, 152501 (2018).

[36] M. Wada, Y. Ishida, T. Nakamura, Y. Yamazaki, T. Kambara, H. Ohyama, Y. Kanai, T. M. Kojima, Y. Nakai, N. Ohshima, A. Yoshida, T. Kubo, Y. Matsuo, Y. Fukuyama, K. Okada, T. Sonoda, S. Ohtani, K. Noda, H. Kawakami, and I. Katayama, Nuclear Instruments and Methods in Physics Research Section B: Beam Interactions with Materials and Atoms **204**, 570 (2003).

[37] A. Takamine, M. Wada, Y. Ishida, T. Nakamura, K. Okada, Y. Yamazaki, T. Kambara, Y. Kanai, T. M. Kojima, Y. Nakai, N. Oshima, A. Yoshida, T. Kubo, S. Ohtani, K. Noda, I. Katayama, P. Hostain, V. Varentsov, and H. Wollnik, Review of Scientific Instruments **76**, 103503 (2005).

[38] G. Bollen, International Journal of Mass Spectrometry **299**, 131 (2011).

[39] F. Arai, Y. Ito, M. Wada, P. Schury, T. Sonoda, and H. Mita, International Journal of Mass Spectrometry **362**, 56 (2014).

[40] W. Xian, M. Rosenbusch, V. Phong, M. Wada, P. Schury, D. Hou, A. Takamine, S. Chen, T. Niwase, Y. Hirayama, *et al.*, Frontiers in Physics **13**, 1644477 (2025).

[41] P. Schury, M. Wada, Y. Ito, F. Arai, S. Naimi, T. Sonoda, H. Wollnik, V. Shchepunov, C. Smorra, and C. Yuan, Nuclear Instruments and Methods in Physics Research Section B: Beam Interactions with Materials and Atoms **335**, 39 (2014).

[42] M. Rosenbusch, Y. Ito, P. Schury, M. Wada, D. Kaji, K. Morimoto, H. Haba, S. Kimura, H. Koura, M. MacCormick, H. Miyatake, J. Y. Moon, K. Morita, I. Murray, T. Niwase, A. Ozawa, M. Reponen, A. Takamine, T. Tanaka, and H. Wollnik, Phys.

Rev. C **97**, 064306 (2018).

[43] J. Park, R. Krücken, D. Lubos, R. Gernhäuser, M. Lewitowicz, S. Nishimura, D. S. Ahn, H. Baba, B. Blank, A. Blazhev, P. Boutachkov, F. Browne, I. Čeliković, G. de France, P. Doornenbal, T. Faestermann, Y. Fang, N. Fukuda, J. Giovinazzo, N. Goel, M. Górska, H. Grawe, S. Ilieva, N. Inabe, T. Isobe, A. Jungclaus, D. Kameda, G. D. Kim, Y.-K. Kim, I. Kojouharov, T. Kubo, N. Kurz, Y. K. Kwon, G. Lorusso, K. Moschner, D. Murai, I. Nishizuka, Z. Patel, M. M. Rajabali, S. Rice, H. Sakurai, H. Schaffner, Y. Shimizu, L. Sinclair, P.-A. Söderström, K. Steiger, T. Sumikama, H. Suzuki, H. Takeda, Z. Wang, H. Watanabe, J. Wu, and Z. Y. Xu, Phys. Rev. C **99**, 034313 (2019).

[44] G. Kripkó-Koncz, W. R. Plaß, I. Dedes, D. D. Dao, T. Dickel, C. Hornung, D. Amanbayev, S. A. S. Andrés, S. Beck, J. Bergmann, A. Blazhev, J. Dudek, H. Geissel, E. Haettner, N. Kalantar-Nayestanaki, I. Mardor, I. Miskun, A. Mollaebrahimi, X. Mougeot, I. Mukha, F. Nowacki, C. Scheidenberger, J. Äystö, S. Bagchi, D. L. Balabanski, A. Baran, i. c. v. Brenčič, V. Charviakova, P. Constantin, M. Dehghan, A. Gaamouci, Z. Ge, M. Górska, L. Gröf, O. Hall, M. N. Harakeh, J.-P. Hucka, A. Kankainen, R. Knöbel, D. A. Kostyleva, N. Kurkova, N. Kuzminchuk, D. Nichita, Z. Patyk, S. Pietri, S. Purushothaman, M. P. Reiter, M. Reponen, H. Roesch, A. Spătaru, G. Stanic, A. State, Y. K. Tanaka, M. c. v. Vencelj, H. Weick, J. Yang, M. I. Yavor, and J. Zhao (for the Super-FRS Experiment Collaboration), Phys. Rev. Res. **7**, L042022 (2025).

[45] M. Phelps and D. Sarantites, Nuclear Physics A **135**, 116 (1969).

[46] O. Koike, M. Hashimoto, K. Arai, and S. Wanajo, Astronomy and Astrophysics **342**, 464 (1999).

[47] A. Dohi, M.-a. Hashimoto, R. Yamada, Y. Matsuo, and M. Y. Fujimoto, Progress of Theoretical and Experimental Physics **2020**, 033E02 (2020).

[48] M. Zhang, Y. Luo, A. Dohi, X. Xu, X. L. Yan, T. Kajino, Y. H. Zhang, and M. Wang, Phys. Rev. C **112**, 065808 (2025).

[49] Y.-Z. Qian and S. Woosley, The Astrophysical Journal **471**, 331 (1996).

[50] K. Otsuki, H. Tagoshi, T. Kajino, and S.-y. Wanajo, The Astrophysical Journal **533**, 424 (2000).

[51] A. Burrows, D. Radice, D. Vartanyan, H. Nagakura, M. A. Skinner, and J. C. Dolence, MNRAS **491**, 2715 (2020).

[52] S. Wanajo, H.-T. Janka, and S. Kubono, The Astrophysical Journal **729**, 46 (2011).